DNA 2776F
AJA-R-7110-2001
December, 1971

SPHERICAL WAVES IN A STRAIN-HARDENING MATERIAL

J. Isenberg
A.K. Bhaumik

Prepared for

DEFENSE NUCLEAR AGENCY
Washington, D. C.

AGBABIAN-JACOBSEN ASSOCIATES
Los Angeles, California

Contract No. DASA01-70-C-0065

DNA 2776F
AJA-R-7110-2001
December, 1971

SPHERICAL WAVES IN A STRAIN-HARDENING MATERIAL

J. Isenberg
A. K. Bhaumik

THIS WORK SPONSORED BY
THE DEFENSE NUCLEAR AGENCY
UNDER NWER SUBTASK SB 047-08

Prepared for

DEFENSE NUCLEAR AGENCY
Washington, D. C.

AGBABIAN-JACOBSEN ASSOCIATES
Los Angeles, California

Contract No. DASA01-70-C-0065

UNCLASSIFIED
Security Classification

DOCUMENT CONTROL DATA - R & D

(Security classification of title, body of abstract and indexing annotation must be entered when the overall report is classified)

1. ORIGINATING ACTIVITY (Corporate author) Agbabian-Jacobsen Associates 8939 S. Sepulveda Boulevard Los Angeles, California 90045	2a. REPORT SECURITY CLASSIFICATION Unclassified 2b. GROUP --

3. REPORT TITLE

Spherical Waves in a Strain-Hardening Material

4. DESCRIPTIVE NOTES (Type of report and inclusive dates)

Final Report

5. AUTHOR(S) (First name, middle initial, last name)

Jeremy Isenberg
Anjan K. Bhaumik

6. REPORT DATE	7a. TOTAL NO. OF PAGES	7b. NO. OF REFS
July 28, 1971	25	3

8a. CONTRACT OR GRANT NO.	9a. ORIGINATOR'S REPORT NUMBER(S)
DASA01-70-C-0065 b. PROJECT NO. NWER Code: XAXS c. Task and Subtask: B047 d. Work Unit: 08	DNA 2776F 9b. OTHER REPORT NO(S) (Any other numbers that may be assigned this report) AJA-R-7110-2001

10. DISTRIBUTION STATEMENT

Approved for public release; distribution unlimited

11. SUPPLEMENTARY NOTES	12. SPONSORING MILITARY ACTIVITY
	Director Defense Nuclear Agency Washington, D. C. 20305

13. ABSTRACT

New constitutive equations are available for earth materials which appear to have theoretical advantages over previous models. The present work extends a previous study of spherical wave progation in inelastic materials to a work-hardening material and compares the results.

DD FORM 1 NOV 68 1473 REPLACES DD FORM 1473, 1 JAN 64, WHICH IS OBSOLETE FOR ARMY USE.

UNCLASSIFIED
Security Classification

CONTENTS

ILLUSTRATIONS

14. KEY WORDS	LINK A		LINK B		LINK C	
	ROLE	WT	ROLE	WT	ROLE	WT
Constitutive equations Spherical wave propagation						

INSTRUCTIONS

1. **ORIGINATING ACTIVITY:** Enter the name and address of the contractor, subcontractor, grantee, Department of Defense activity or other organization *(corporate author)* issuing the report.

2a. **REPORT SECURITY CLASSIFICATION:** Enter the overall security classification of the report. Indicate whether "Restricted Data" is included. Marking is to be in accordance with appropriate security regulations.

2b. **GROUP:** Automatic downgrading is specified in DoD Directive 5200.10 and Armed Forces Industrial Manual. Enter the group number. Also, when applicable, show that optional markings have been used for Group 3 and Group 4 as authorized.

3. **REPORT TITLE:** Enter the complete report title in all capital letters. Titles in all cases should be unclassified. If a meaningful title cannot be selected without classification, show title classification in all capitals in parenthesis immediately following the title.

4. **DESCRIPTIVE NOTES:** If appropriate, enter the type of report, e.g., interim, progress, summary, annual, or final. Give the inclusive dates when a specific reporting period is covered.

5. **AUTHOR(S):** Enter the name(s) of author(s) as shown on or in the report. Enter last name, first name, middle initial. If military, show rank and branch of service. The name of the principal author is an absolute minimum requirement.

6. **REPORT DATE:** Enter the date of the report as day, month, year; or month, year. If more than one date appears on the report, use date of publication.

7a. **TOTAL NUMBER OF PAGES:** The total page count should follow normal pagination procedures, i.e., enter the number of pages containing information.

7b. **NUMBER OF REFERENCES:** Enter the total number of references cited in the report.

8a. **CONTRACT OR GRANT NUMBER:** If appropriate, enter the applicable number of the contract or grant under which the report was written.

8b, 8c, & 8d. **PROJECT NUMBER:** Enter the appropriate military department identification, such as project number, subproject number, system numbers, task number, etc.

9a. **ORIGINATOR'S REPORT NUMBER(S):** Enter the official report number by which the document will be identified and controlled by the originating activity. This number must be unique to this report.

9b. **OTHER REPORT NUMBER(S):** If the report has been assigned any other report numbers *(either by the originator or by the sponsor)*, also enter this number(s).

10. **AVAILABILITY/LIMITATION NOTICES:** Enter any limitations on further dissemination of the report, other than those imposed by security classification, using standard statements such as:

(1) "Qualified requesters may obtain copies of this report from DDC."

(2) "Foreign announcement and dissemination of this report by DDC is not authorized."

(3) "U. S. Government agencies may obtain copies of this report directly from DDC. Other qualified DDC users shall request through _____."

(4) "U. S. military agencies may obtain copies of this report directly from DDC. Other qualified users shall request through _____."

(5) "All distribution of this report is controlled. Qualified DDC users shall request through _____."

If the report has been furnished to the Office of Technical Services, Department of Commerce, for sale to the public, indicate this fact and enter the price, if known.

11. **SUPPLEMENTARY NOTES:** Use for additional explanatory notes.

12. **SPONSORING MILITARY ACTIVITY:** Enter the name of the departmental project office or laboratory sponsoring *(paying for)* the research and development. Include address.

13. **ABSTRACT:** Enter an abstract giving a brief and factual summary of the document indicative of the report, even though it may also appear elsewhere in the body of the technical report. If additional space is required, a continuation sheet shall be attached.

It is highly desirable that the abstract of classified reports be unclassified. Each paragraph of the abstract shall end with an indication of the military security classification of the information in the paragraph, represented as *(TS), (S), (C), or (U)*.

There is no limitation on the length of the abstract. However, the suggested length is from 150 to 225 words.

14. **KEY WORDS:** Key words are technically meaningful terms or short phrases that characterize a report and may be used as index entries for cataloging the report. Key words must be selected so that no security classification is required. Identifiers, such as equipment model designation, trade name, military project code name, geographic location, may be used as key words but will be followed by an indication of technical context. The assignment of links, rules, and weights is optional.

ILLUSTRATIONS (CONTINUED)

TABLES

SUMMARY

New constitutive relations for earth materials are available which appear to have theoretical advantages over previous mathematical models. The present work applies the new model, which is adapted to a tonalite, to numerical computations of spherical wave propagation. Parameters such as attenuation rates, stress trajectories and displacement of the cavity wall are compared with similar parameters obtained from numerical computations using different mathematical models of the same material. Except for the displacement of the cavity wall, the new model leads to results which are similar to those found by the most advanced of the previous models.

FOREWORD

The work reported here was conducted under NWER Subtask SB047, work unit 38, between February and July 1971. The DNA monitor was Mr. C. B. McFarland, Jr.

SECTION 1

INTRODUCTION

New constitutive equations are available for Cedar City tonalite which appear to have theoretical advantage over some previous models (Reference 1). The present analysis extends the work of Reference 2 by using this model to calculate spherical wave propagation. A comparison is made between the models considered in Reference 2 and the new "capped" model, on the basis of attenuation rates, stress/time histories, cavity growth, and rate of energy absorption. An adaptation of the capped model is reported which appears to be stable, convergent, and applicable to both finite element and finite difference methods in continuum mechanics.

The present calculations are performed in the manner described in Reference 2. The finite element method is adapted to spherical geometry. The mathematical model of Cedar City tonalite reported in Reference 1 is modified such that the shear modulus, hydrostat, and yield criteria are as close to those used in Reference 2 as the different forms of the various models permit. The tonalite is considered to be an infinite medium surrounding a cavity which contains a sphere of chemical explosive. Detonation of the explosive is represented by applying pressure to the surface of the cavity which leaves with time in a manner similar to that measured by Physics International Company (Reference 3) in physical experiments. The peak pressure at the cavity wall is 31.5 kb.

The results of the calculations are presented as stress/time histories and stress/strain relations at various ranges and as rates of attenuation of the peak radial stress. The main question to be investigated is whether using the device of strain hardening to incorporate volumetric hysteresis dramatically affects the wave shape, the attenuation rate, or the cavity growth. The findings indicate that, at least in spherical wave propagation, the "capped" model leads to approximately the same results as found using the best of the previous models.

SECTION 2

FINITE ELEMENT ADAPTATION OF THE CAPPED MODEL FOR ROCK

The model consists of an ideally plastic modified Drucker-Prager yield criterion,

$$f_1\left(J_1, \sqrt{J_2'}\right) = 0 \quad \ldots\ldots\ldots\ldots\ldots\ldots \quad (2\text{-}1)$$

and a cap.

$$f_2\left(J_1, \sqrt{J_2'}, \kappa\right) = 0 \quad \ldots\ldots\ldots\ldots\ldots \quad (2\text{-}2)$$

where J_1 is the first stress invariant, J_2' is the second invariant of the stress deviators, and κ is a given function of the stress-strain history of the rock. A variable bulk modulus model which is a function of J_1 and a constant shear modulus are used. The plastic potential flow rule is used to determine plastic strain rates on both f_1 and f_2.

YIELD FUNCTIONS--FRACTURE SURFACE AND CAP

From experimental data on Cedar City Tonalite, Sandler and Dimaggio proposed the following functions for f_1 and f_2:

$$f_1 = \sqrt{J_2'} - 152 + 145e^{0.0029\, J_1} = 0 \quad \ldots\ldots \quad (2\text{-}3)$$

$$f_2 = \frac{(J_1 - J_c)^2}{R^2} + J_2' - Q = 0 \quad \ldots\ldots\ldots \quad (2\text{-}4)$$

where J_1 and J_2' are expressed in ksi. The quantities J_c, R and Q are functions of the cap parameter κ. With reference to Figure 2-1, J_c is the value of J_1 at the center C of the elliptical cap, R is the ratio of the major to minor axes, and Q is the value of J_2' on the cap when $J_1 = J_c$. To ensure tangency at the junction F of f_1 and f_2, these quantities are determined as follows:

$$J_c = J_{1F} - R^2 \sqrt{J'_{2F}} \left(\frac{\partial f_1 / \partial J_1}{\partial f_1 / \partial \sqrt{J'_2}} \bigg|_F \right) \quad \ldots\ldots\ldots \quad (2\text{-}5)$$

$$Q = J'_{2F}\, 1 + R^2 \left(\frac{\partial f_1 / \partial J_1}{\partial f_1 / \partial \sqrt{J'_2}} \bigg|_F \right)^2 \quad \ldots\ldots\ldots \quad (2\text{-}6)$$

where

$$J'_{2F} = 152 - 145e^{0.0029\, J_{1F}} \quad \ldots\ldots\ldots\ldots \quad (2\text{-}7)$$

$$J_{1F} = -450\kappa \quad \ldots\ldots\ldots\ldots\ldots\ldots \quad (2\text{-}8)$$

$$R = 4.0e^{-0.05\, J_{1F}} \quad \ldots\ldots\ldots\ldots\ldots \quad (2\text{-}9)$$

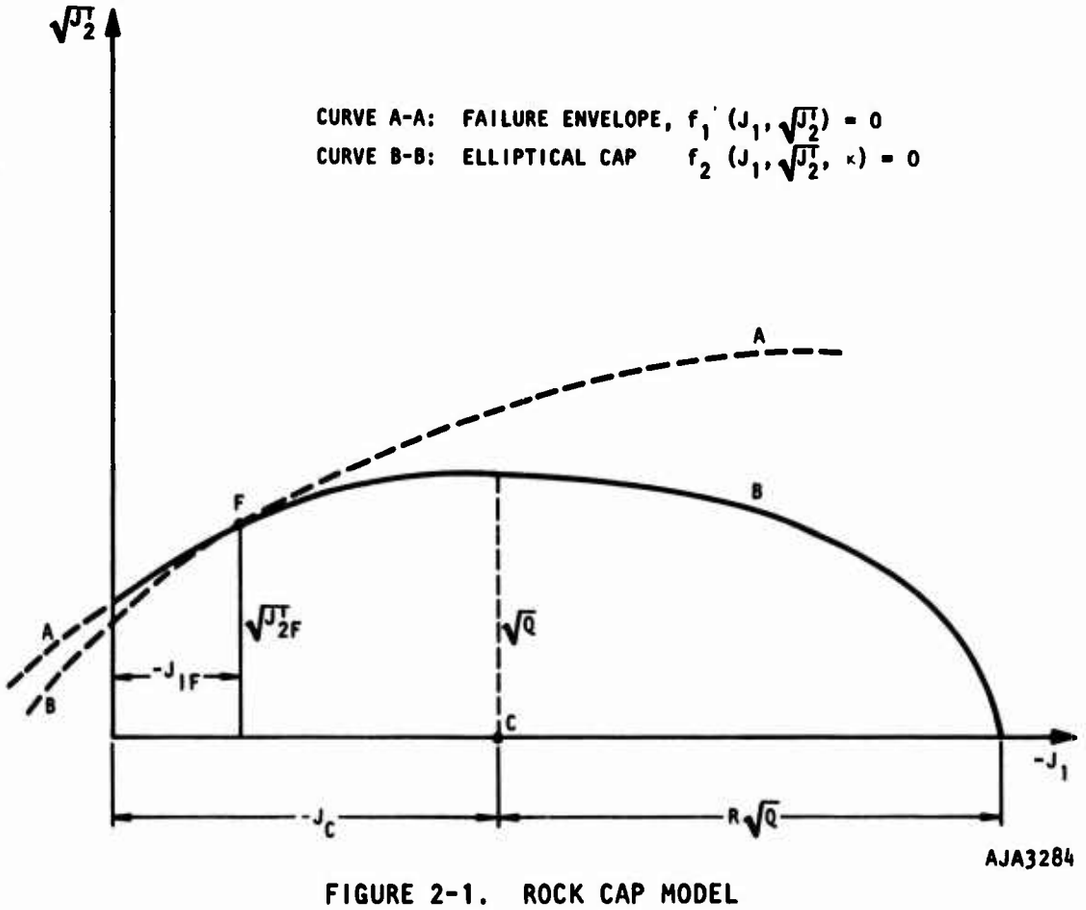

FIGURE 2-1. ROCK CAP MODEL

The cap parameter κ is defined by

$$\kappa = \sum - f_1\sqrt{\left(d\varepsilon_{11}^{p\ell}\right)^2 + \left(d\varepsilon_{22}^{p\ell}\right)^2 + \left(d\varepsilon_{33}^{p\ell}\right)^2} \quad \ldots \quad (2\text{-}10)$$

where $d\varepsilon_{11}^{p\ell}$, $d\varepsilon_{22}^{p\ell}$, and $d\varepsilon_{33}^{p\ell}$ are the principal components of the plastic strain increments.

BULK AND SHEAR MODULI

The bulk modulus B is a function of mean stress as follows:

$$B = B_1\left(1 - B_2 e^{B_3 J_1}\right) \quad \ldots \quad (2\text{-}11)$$

The shear modulus μ is a constant.

$$\mu = \text{constant} \quad \ldots \quad (2\text{-}12)$$

INCREMENTAL STRESS/STRAIN RELATIONSHIP

For small strain increments, the incremental stress tensor, $d\sigma_{ij}$, is related to total strain increment $d\varepsilon_{ij}$ and the plastic strain increment $d\varepsilon_{ij}^{p\ell}$ as follows:

$$d\sigma_{ij} = \lambda\left(d\varepsilon_{kk} - d\varepsilon_{kk}^{p\ell}\right)\delta_{ij} + 2\mu\left(d\varepsilon_{ij} - d\varepsilon_{ij}^{p\ell}\right) \quad \ldots \quad (2\text{-}13)$$

where λ and μ are Lame's constants, δ_{ij} is the Kronecker delta, and the sum of the elastic and plastic parts is the total strain increment.

The yield function can be expressed as

$$f(\sigma_{ij}, \kappa) = 0 \quad \ldots \quad (2\text{-}14)$$

where κ is the cap parameter defined in Equation 2-10. It is to be noted here that the failure envelope is a function of the

stresses and the cap parameter. An associated flow rule is used in conjunction with the capped yield surface, i.e.,

$$d\varepsilon_{ij}^{p} = \Lambda \frac{\partial f}{\partial \sigma_{ij}} \quad \ldots\ldots\ldots\ldots\ldots\ldots \quad (2\text{-}15)$$

where Λ is a scalar to be determined.

During inelastic deformation, the total differential of the yield function is equal to zero. Thus,

$$df = f_{ij} d\sigma_{ij} + f_{\kappa} d\kappa = 0 \quad \ldots\ldots\ldots\ldots \quad (2\text{-}16)$$

where

$$f_{ij} = \frac{\partial f}{\partial \sigma_{ij}}$$

and

$$f_{\kappa} = \frac{\partial f}{\partial \kappa} .$$

The expression $d\kappa$ can be obtained from Equation 2-10 as

$$d\kappa = -f_1 \sqrt{\left(d\varepsilon_{11}^{p\ell}\right)^2 + \left(d\varepsilon_{22}^{p\ell}\right)^2 + \left(d\varepsilon_{33}^{p\ell}\right)^2} \quad \ldots\ldots \quad (2\text{-}17)$$

Substituting Equation 15 in Equation 2-17 and Equation 2-13, the following relations are obtained.

$$d\kappa = -\Lambda f_1 \sqrt{f_{11}^2 + f_{22}^2 + f_{33}^2} \quad \ldots\ldots\ldots\ldots \quad (2\text{-}18)$$

and

$$d\sigma_{ij} = \lambda\, d\varepsilon_{kk}\delta_{ij} + 2\mu\, d\varepsilon_{ij} - \Lambda\left(\lambda f_{kk}\delta_{ij} + 2\mu\delta_{ij}\right) \quad . \quad (2\text{-}19)$$

Substitution of Equations 2-18 and 2-19 in Equation 2-16 yields

$$\lambda\, d\varepsilon_{kk} f_{\ell\ell} + 2\mu\, d\varepsilon_{ij} f_{ij} - \Lambda\left\{\lambda\left(f_{kk}\right)^2 + 2\mu\, f_{ij} f_{ij} + f_1 f_\kappa \sqrt{f_{11}^2 + f_{22}^2 + f_{33}^2}\right\} \quad \ldots \quad (2\text{-}20)$$

The scalar Λ is obtained from Equation 2-20.

$$\Lambda = \frac{\lambda\, d\varepsilon_{kk} f_{\ell\ell} + 2\mu\, d\varepsilon_{ij} f_{ij}}{\lambda\left(f_{kk}\right)^2 + 2\mu\, f_{ij} f_{ij} + X} \quad \ldots \quad (2\text{-}21)$$

where

$$X = f_1 f_\kappa \sqrt{f_{11}^2 + f_{22}^2 + f_{33}^2} \quad \ldots \quad (2\text{-}22)$$

Substitution of Equation 2-21 into Equation 2-19 yields the desired incremental stress/strain relationship. Adjusting the tensorial shear strain ε_{ij} to the engineering shear strain γ_{ij}, the following stress/strain relationship is obtained.

$$\begin{Bmatrix} d\sigma_{rr} \\ d\sigma_{zz} \\ d\sigma_{\theta\theta} \\ d\sigma_{rz} \end{Bmatrix} = \begin{bmatrix} \lambda + 2\mu - \frac{Y_r^2}{D} & \lambda - \frac{Y_r Y_z}{D} & \lambda - \frac{Y_r Y_\theta}{D} & -2\mu \frac{f_{rz} Y_r}{D} \\ & \lambda + 2\mu - \frac{Y_z^2}{D} & \lambda - \frac{Y_z Y_\theta}{D} & -2\mu \frac{f_{rz} Y_z}{D} \\ & \text{Symmetrical} & \lambda + 2\mu - \frac{Y_\theta^2}{D} & -2\mu \frac{f_{rz} Y_\theta}{D} \\ & & & \mu - \frac{4\mu^2 f_{rz}^2}{D} \end{bmatrix} \begin{Bmatrix} d\varepsilon_{rr} \\ d\varepsilon_{zz} \\ d\varepsilon_{\theta\theta} \\ d\gamma_{rz} \end{Bmatrix} \quad (2\text{-}23)$$

where

$$F = \frac{\partial f}{\partial \sigma_{rr}} + \frac{\partial f}{\partial \sigma_{\theta\theta}} + \frac{\partial f}{\partial \sigma_{zz}}$$

$$f_{rz} = \frac{\partial f}{\partial \sigma_{rz}}$$

$$Y_r, \text{ etc.} = \lambda F + 2\mu \frac{\partial f}{\partial \sigma_{rr}}$$

$$D = \lambda F^2 + 2\mu\left(f_{rr}^2 + f_{\theta\theta}^2 + f_{zz}^2\right) + f_1 f_k \sqrt{f_{rr}^2 + f_{\theta\theta}^2 + f_{zz}^2}$$

Equation 2-22 is the instantaneous incremental stress/strain relation for small strain increments. An iterative scheme (Figure 2-2), similar to the modified Euler formula, is employed to obtain stress increments for finite increments of strain.

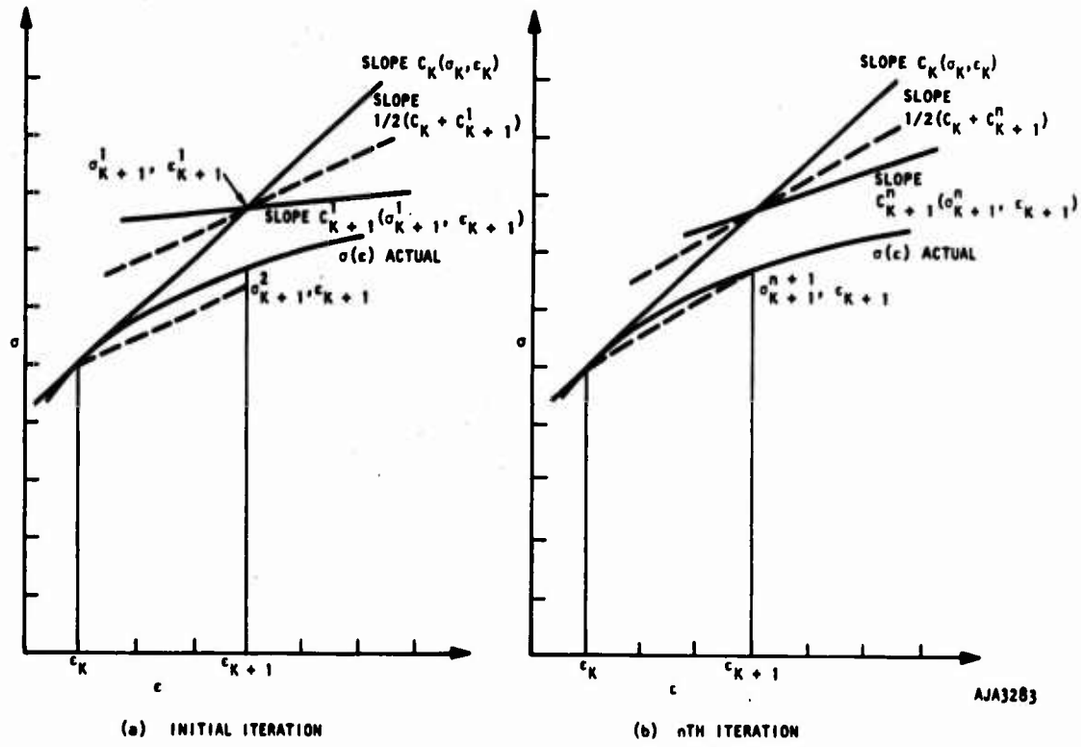

FIGURE 2-2. ITERATION SCHEME TO EVALUATE STRESSES

The procedure to obtain the stress increment during a step is described below.

$$\{\Delta\sigma\}_{k+1} = \frac{1}{2}\left\{[C]_k + [C]_{k+1}\right\}\{\Delta\varepsilon\}_{k+1} \quad \ldots\ldots\ldots \quad (2\text{-}24)$$

where $[C]_k$ and $[C]_{k+1}$ are the instantaneous stress/strain relationships at the beginning and the end of the step, respectively. Since $[C]_{k+1}$ depends on the stresses at the end of the time step, successive corrections to $[C]_{k+1}$ and to $\{\Delta\sigma\}_{k+1}$ are made until the following function of stress increments reaches a stationary value within a prescribed tolerance:

$$E = |\Delta\sigma_1| + |\Delta\sigma_2| + |\Delta\sigma_3| \quad \ldots\ldots\ldots\ldots \quad (2\text{-}25)$$

SECTION 3

NUMERICAL RESULTS

Calculations were performed in which a pressure/time history is applied to the surface of a spherical cavity in an infinite medium. The finite element grid that represents the medium and the cavity is shown in Figure 3-1. The pressure/time history applied to the surface of the cavity is also shown.

A series of eight calculations has been performed to study the influence on spherical wave propagation of such material parameters as volumetric hysteresis and plastic dilatency. The purpose of this study was to determine which aspects of a material model most strongly affect calculations of wave propagation and thus require the most complete experimental determination. The first seven calculations (Cases 1 through 7), which explore a range of mathematical models from linearly elastic through variable modulus with plasticity, are reported in Reference 2. The eighth calculation (Case 8), reported below considers an elastic/plastic model with a strain hardening cap whose purpose is to provide plastic volumetric compaction within the general framework of plasticity theory. Table 3-1 summarizes the material properties considered in Cases through 8.

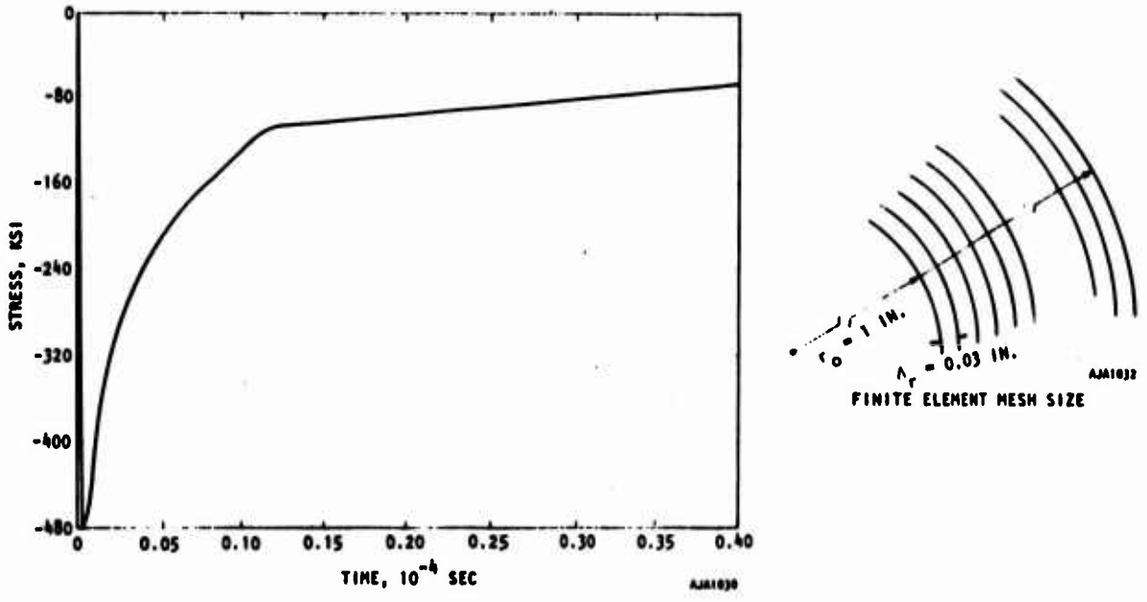

FIGURE 3-1. MESH SIZE AND LOADING USED IN CALCULATIONS

TABLE 3-1. SUMMARY OF MATERIAL PROPERTIES AND LOADING USED IN SPHERICAL WAVE CALCULATIONS

Case	Description
1	Linear elastic (no yield condition imposed); $B = B_o = 1.2 \times 10^6$ psi; $G = 1 \times 10^6$ psi
2	Variable modulus (no yield condition imposed); B defined in Table 3-2; $G = 1 \times 10^6$ psi
3	Variable modulus as in Case 2 with von Mises yield criterion ($\alpha = 0$, $c = 76{,}125$ psi)
4	Variable modulus as in Case 4 with Coulomb yield criterion ($\alpha = -0.167$, $c = 1450$ psi) at $p > -14.5$ kb and von Mises criterion ($\alpha = 0$, $c = 76{,}125$ psi) at $p < -14.5$ kb. Plastic Potential flow rule is used.
5	Same as Case 4, except that Prandlt-Reuss flow rule is used.
6	Same as Case 4, except that impulse is increased by a factor of 2.
7	Same as Case 2, except that impulse is increased by a factor of 2.
8	Yield criterion, bulk and shear moduli similar to Cases 4 and 5, except that capped model is used to represent volumetric hysteresis.

NOTE: Cases 1 through 7 are previous analyses; Case 8 is the present analysis.

The yield criteria and hydrostatic stress/strain properties of the material model in Cases 4, 5, and 8 are similar as indicated in Table 3-2 and Figures 3-2 and 3-3. However, the mathematical formulation of the capped model (Case 8) differs significantly from that of the other two. The models in Cases 4, 5, and 8 and known to be similar only for certain stress paths. Differences may occur when the material is subjected to other stress paths. The subject which is investigated below is whether the differences in mathematical formulation lead to differences in the response to spherical wave propagation.

TABLE 3-2. SUMMARY OF MATERIAL PROPERTIES

	Case 4 and Case 5	Case 8 Adaptation of Dimaggio-Sandler Model
Shear Modulus	$G = 1.0 \times 10^6$ psi	$G = 1.0 \times 10^6$ psi
Bulk Modulus	Loading ($\mu \geq \mu_{max}$, the previous maximum μ) $B = B_1 - (B_1 - B_o) \exp - \frac{\mu}{\mu_1}$ unloading/reloading ($\mu < \mu_{max}$) $B = B_u + (B_1 - B_u) \frac{\mu}{\mu_2}$ where B_u = the lesser of $\begin{cases} B_o + (B_1 - B_o) \frac{\mu_{max}}{\mu_2} \\ B_1 \end{cases}$ with $B_1 = 7.6 \times 10^6$ psi $B_o = 1.205 \times 10^6$ psi $\mu_1 = 0.0275$ $\mu_2 = 0.05$ $\mu = \varepsilon_r^{pl} + \varepsilon_\theta^{pl} + \varepsilon_\phi^{pl}$	$B = B_1\ 1.0 - B_2\, e^{B_3 J_1}$ with $B_1 = 7.6 \times 10^6$ psi $B_2 = 0.84$ $B_3 = 0.47 \times 10^{-5}$ $J_1 = \sigma_r + \sigma_\phi + \sigma_\theta$ (psi)
Yield Function	$\sqrt{J_2'} = -0.167\, J_1 + 1450$ psi for $J_1 \geq -448{,}050$ psi $\sqrt{J_2'} = 76{,}000$ psi for $J_1 < -448{,}050$ psi	<u>Failure Curve</u> $f_1 = \sqrt{J_2'} - 76{,}000 + 74{,}550 \exp(0.224 \times 10^{-5} J_1) = 0$ <u>Cap</u> $f_2 = \left(\frac{J_1 - J_c}{R}\right)^2 + J_2' - Q = 0$ where $J_c = J_{1F} - R^2 \sqrt{J_{2F}'} \left(\frac{\partial f_1/\partial J_1}{\partial f_1/\partial \sqrt{J_2'}} \Big|_F \right)$ $Q = J_{2F}' \left[1 + R^2 \left(\frac{\partial f_1/\partial J_1}{\partial f_1/\partial \sqrt{J_2'}} \Big|_F \right)^2 \right]$ $\sqrt{J_{2F}'} = 76{,}000 - 74{,}500 \exp(0.229 \times 10^{-5} J_{1F})$ (psi) $J_{1F} = -450\kappa$ $\kappa = \sum - f_1 \left[\left(d\varepsilon_r^{pl}\right)^2 + \left(d\varepsilon_\theta^{pl}\right)^2 + \left(d\varepsilon_\phi^{pl}\right)^2 \right]^{1/2}$ $R = 4.0 \exp(-0.5 \times 10^{-4} J_{1F})$
Flow Rule	Case 4 - Plastic potential Case 5 - Prandtl-Reuss	Plastic potential

AJA3298

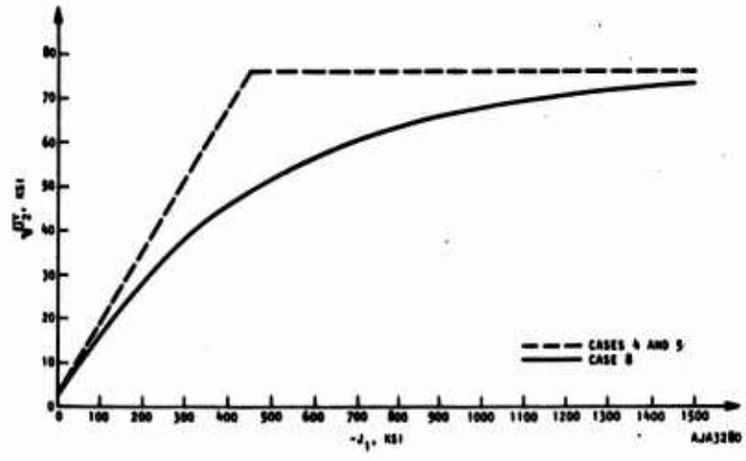

FIGURE 3-2. FAILURE CURVE (CASE 8) AND YIELD FUNCTION (CASES 4 AND 5)

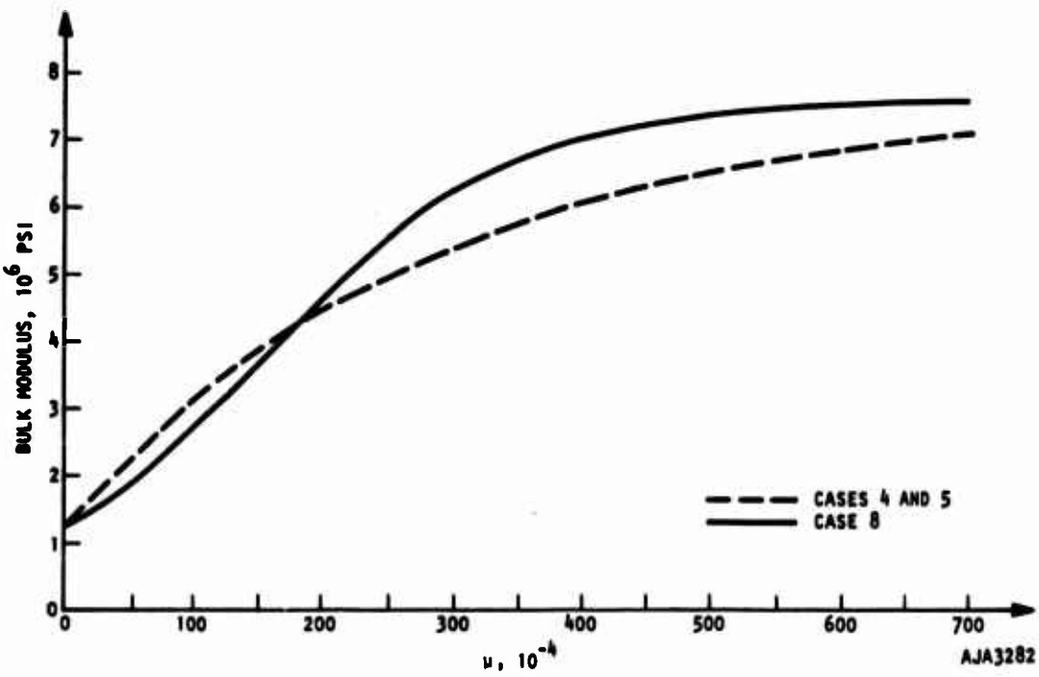

(a) BULK MODULUS VERSUS VOLUMETRIC STRAIN, CASES 4, 5 AND 8

FIGURE 3-3. BULK MODULUS AND HYDROSTAT USED IN CASE 8 ARE PRESCRIBED BY DIFFERENT FORMULAS BUT HAVE NEARLY THE SAME VALUES AS IN PREVIOUS CASES

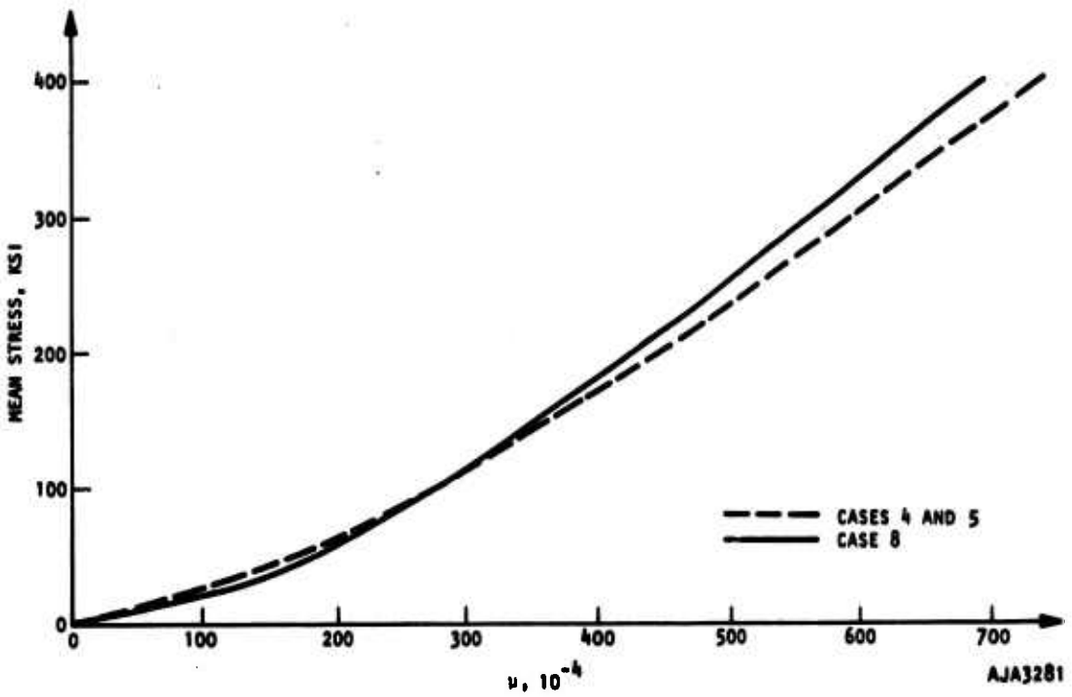

(b) HYDROSTAT, CASES 4, 5 AND 8

FIGURE 3-3. (CONTINUED)

SECTION 4

RESULTS OF CALCULATIONS

STRESS/TIME HISTORIES

The radial and circumferential stress/time histories for Cases 4, 5, and 8 are shown in Figure 4-1. Compressive stresses are defined as negative.

Cases 4 and 8 are similar in that the circumferential stresses remain compressive throughout the duration of the calculation. They differ from Case 5 in this respect for the following reason. The yield criteria have a Coulomb portion which allows plastic deformation to occur at all ranges considered in the three cases. The materials of Cases 4 and 8 exhibit dilatency, or volumetric expansion, which tends to induce lateral compressive stresses. This tendency is partly counteracted by outward radial displacement, which contributes to lateral tensile stresses. Dilatency dominates in Cases 4 and 8, however, in that tensile hoop stresses do not develop. In Case 5, no dilatency is allowed, and hence tensile stresses develop.

STRESS TRAJECTORIES

The stress history in terms of σ_r versus σ_θ, σ_ϕ is referred to below as a stress trajectory. Trajectories at r/r_o = 1, 2, 3, and 4 are shown in Figures 4-2 through 4-5. The loading is initially elastic up to about J_1 = -7 Kb. Loading continues on the cap up to the peak values of σ_r and σ_θ, σ_ϕ. Unloading is initially elastic in the region where oscillations occur. As unloading continues, the stress point again encounters the cap. At r/r_o = 3 and 4, the stress point remains on the cap throughout the duration unloading. At r/r_o = 1, the stress point spends only a brief time on the cap and then moves onto the fracture surface. At r/r_o = 2, the stress point is primarily in the elastic region and on the cap and moves onto the fracture surface only near the end of the calculation.

During initial loading, the cap moves rapidly away from the origin. In this phase there is at some stages plastic volumetric compaction and at other stages plastic volumetric expansion. There is also some plastic shear strain. During unloading on the cap, the sense of the plastic volume strain is exclusively expansion. The motion of the cap during unloading is small compared with that during loading. This is because changes in the cap parameter depend on f_1 (see Equation 2-10), which tends toward zero as the stress point approaches the fracture surface.

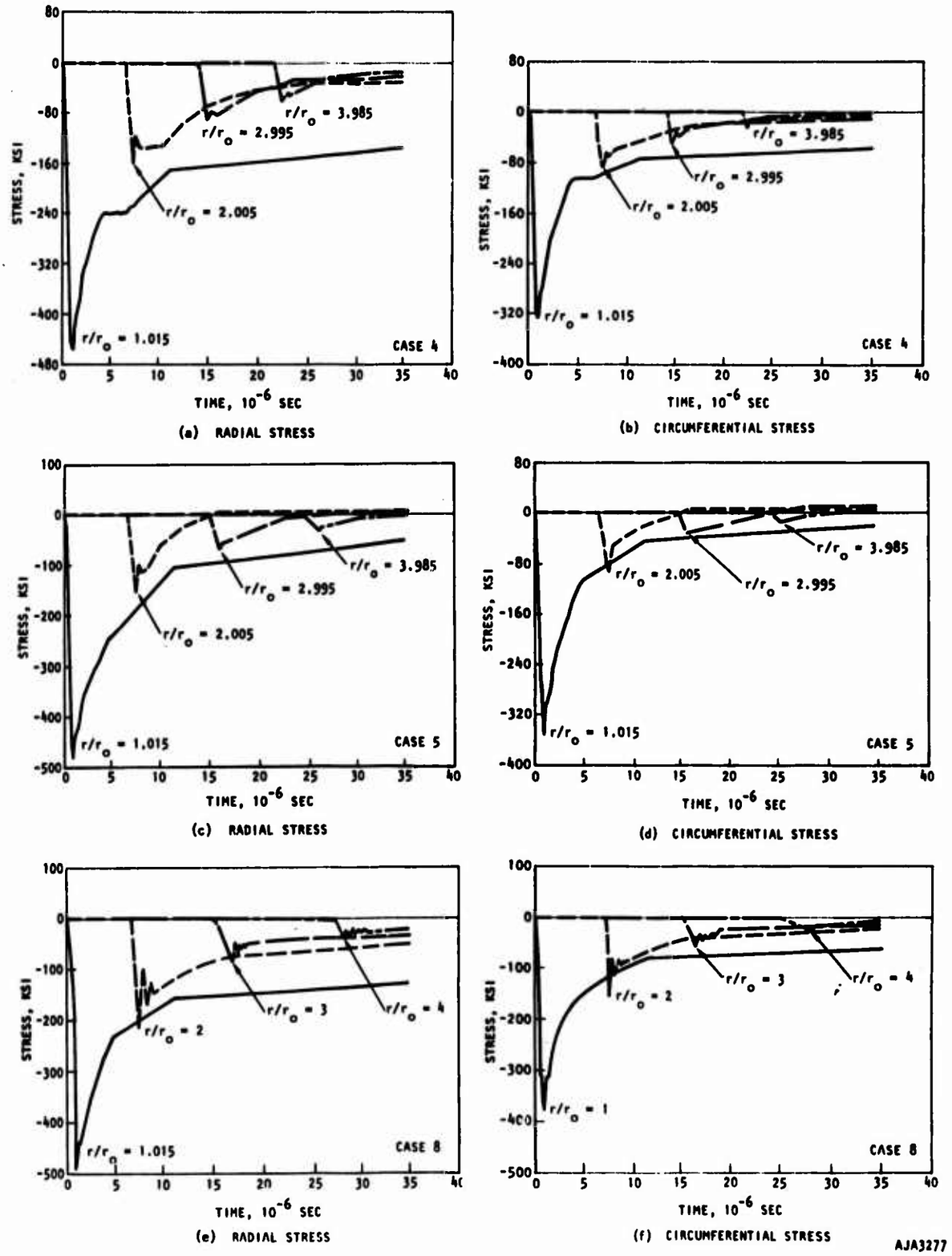

FIGURE 4-1. STRESS/TIME HISTORIES, CASES 4, 5 AND 8

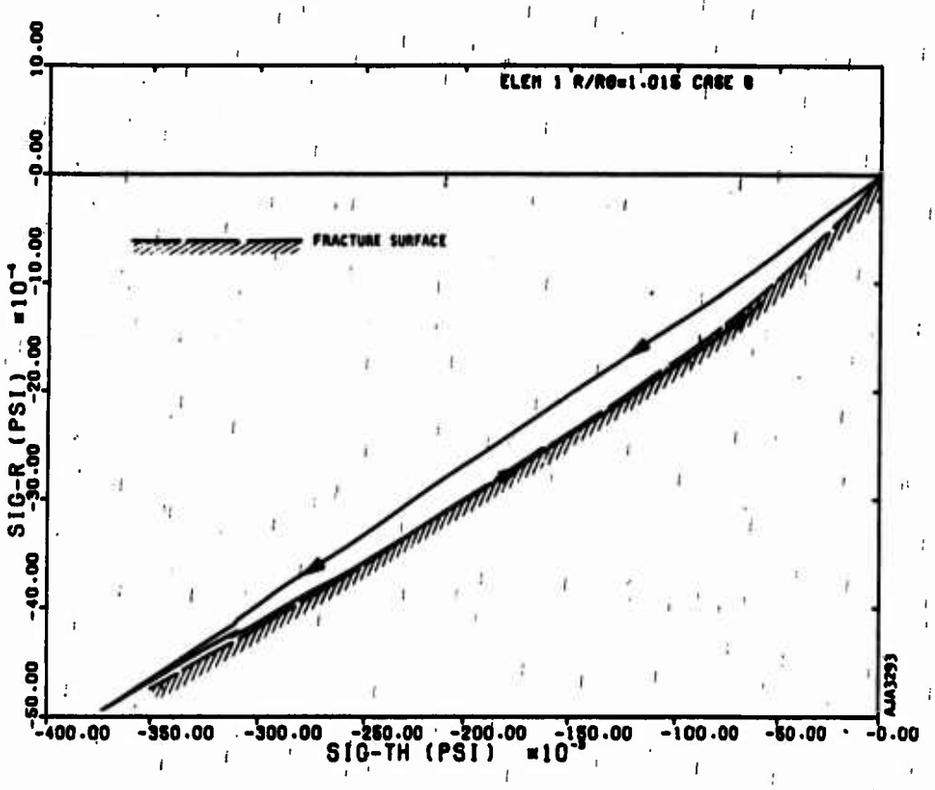

FIGURE 4-2. STRESS TRAJECTORY AT r/r_o = 1.015 (ELEMENT ADJACENT TO CAVITY)

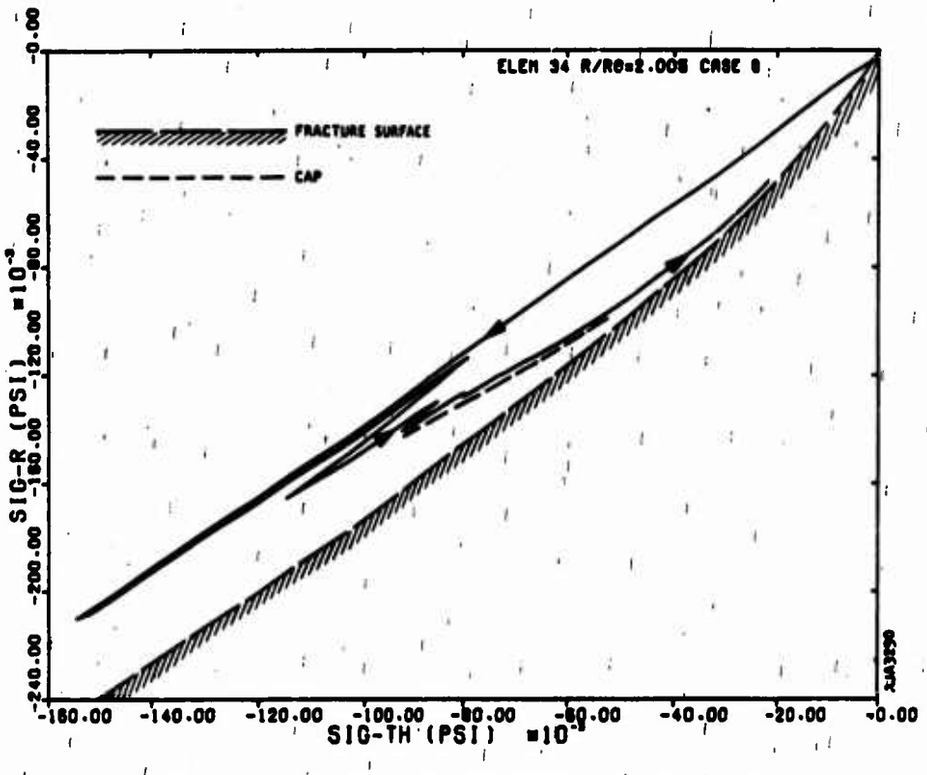

FIGURE 4-3. STRESS TRAJECTORY AT r/r_o = 2

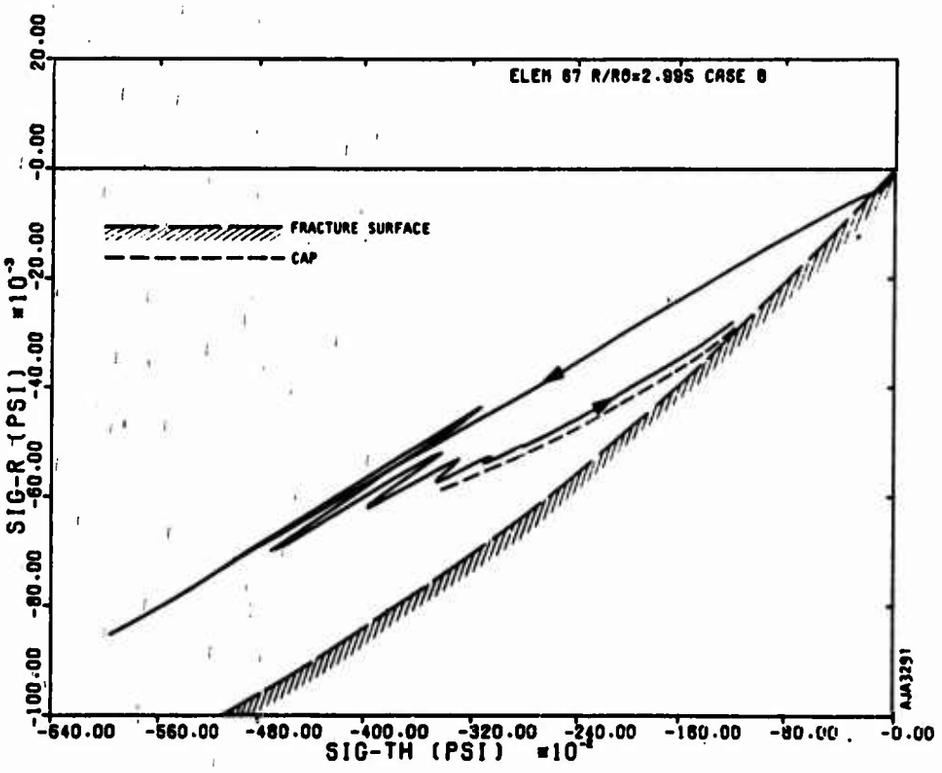

FIGURE 4-4. STRESS TRAJECTORY AT $r/r_o = 3$

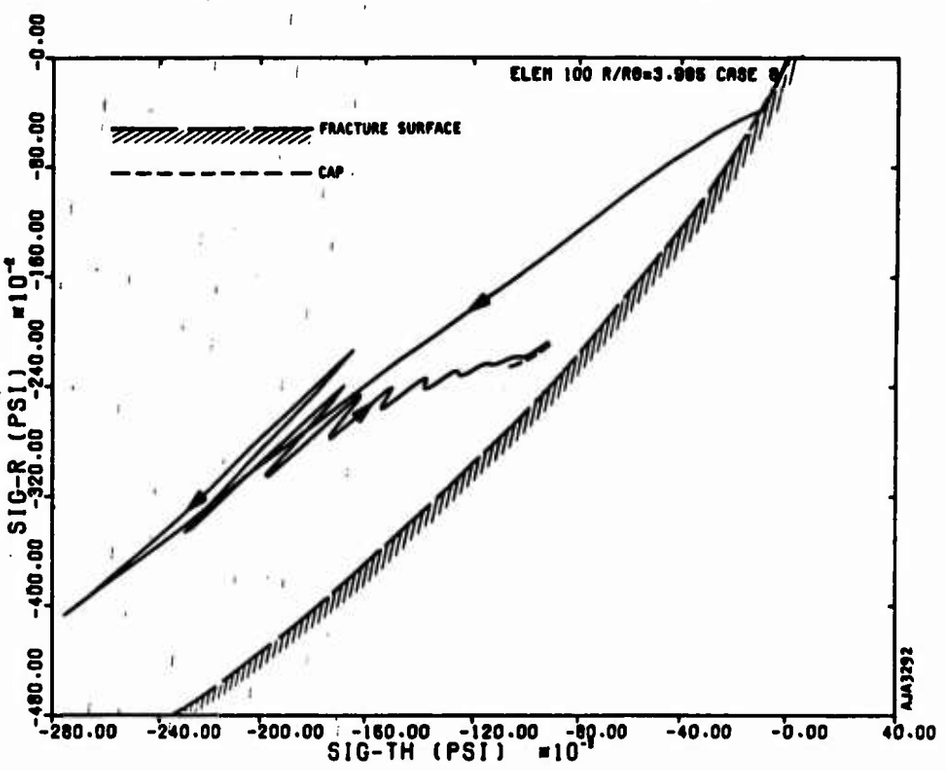

FIGURE 4-5. STRESS TRAJECTORY AT $r/r_o = 4$

DILATENCY AND τ/γ

In Reference 2, an analysis was made of inelastic energy absorption at several ranges. In Case 4 it was found that dilatency, which arises from using the plastic potential flow rule combined with yield criterion, produces a net volumetric expansion. It is suggested that one effect of dilatency is to reduce the unloading wave velocity, and that this is why the peak radial stress attenuates more slowly in Case 4 than in Cases 2 and 5 (no dilatency).

To investigate this subject for the capped model, plots of pressure versus excess compression (P/μ) and shear stress versus shear strain (τ/γ) were prepared and are shown in Figures 4-6 and 4-7. A main finding of Case 8 is that there is net dilatency at $r/r_o = 2$ and 3 (Figure 4-6(c)), just as there is in Case 4. Although it is difficult to define the term "amount of dilatency," there would appear to be less in Case 8 than in Case 4. If this is true, of the three cases in Figure 4-6, Case 4 has the greatest amount of dilatency, Case 8 is intermediate, and Case 5 has none. This is a useful observation in interpreting the attenuation rates.

ATTENUATION RATES

The rates at which peak radial stresses attenuate with range in Cases 4, 5, and 8 are shown in Figure 4-8. Beyond $r/r_o = 2.5$ the attenuation rate in Case 8 is intermediate between Cases 4 and 5. Thus, as in the previous cases, the attenuation rate appears to be correlated with the amount of dilatency and hence the speed of unloading signals.

GROWTH OF CAVITY

The displacements of the cavity wall for Cases 4, 5, and 8 are shown in Figure 4-9. The relative magnitudes of the displacements reflect important aspects of material behavior. Up until 5×10^{-6} sec, the displacement in Cases 4 and 5 are similar. However, as soon as unloading proceeds to where the stress point is on the yield surface, dilatency develops in Case 4 and does not develop in Case 5. Since dilatency tends to retard cavity growth, the cavity grows more rapidly in Case 5 than in Case 4.

The reason for greater cavity growth in Case 8 is partly due to the fact that plastic shear strains occur on loading as a result of using the plastic potential flow rule in conjunction with the cap. This cannot be the full explanation, however. The reason cited above should affect displacements more at early than

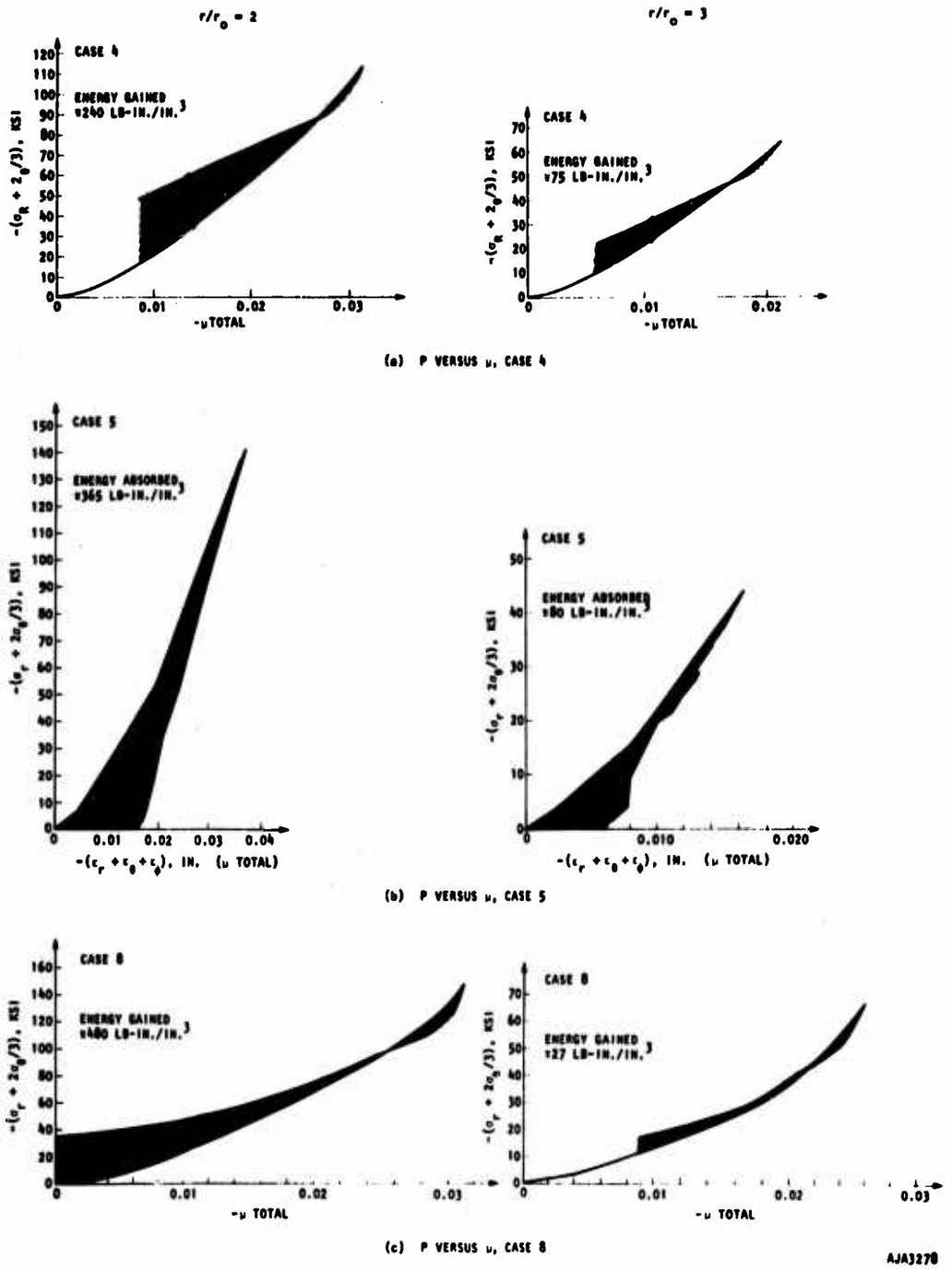

FIGURE 4-6. PRESSURE VERSUS VOLUMETRIC STRAIN AT $r/r_o = 2$ AND $r/r_o = 3$ FOR CASES 4, 5 AND 8

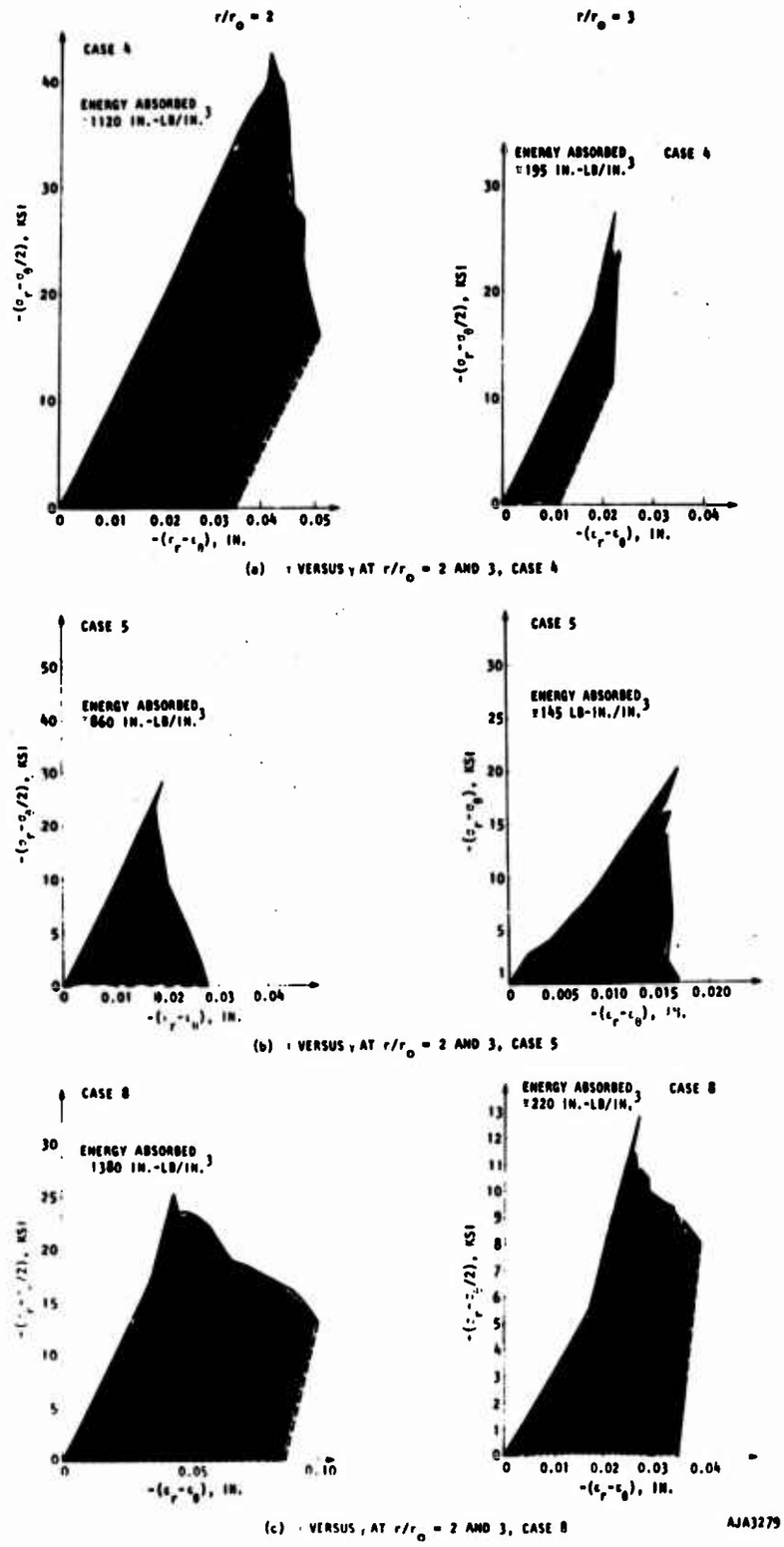

FIGURE 4-7. SHEAR STRESS/STRAIN CURVES AT $r/r_o = 2$ AND $r/r_o = 3$ FOR CASES 4, 5 AND 8

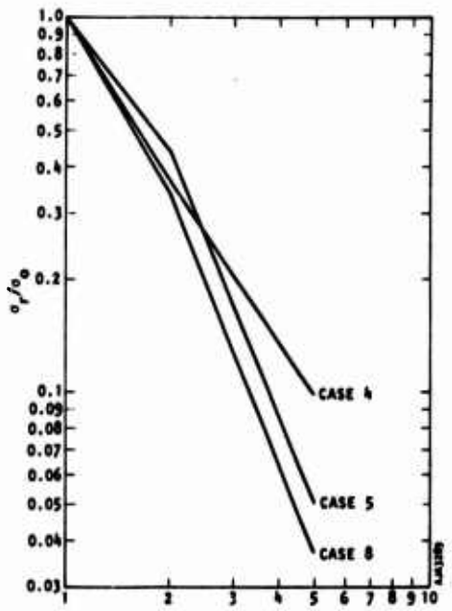

FIGURE 4-8. ATTENUATION OF PEAK RADIAL STRESS, CASES 4, 5 AND 8

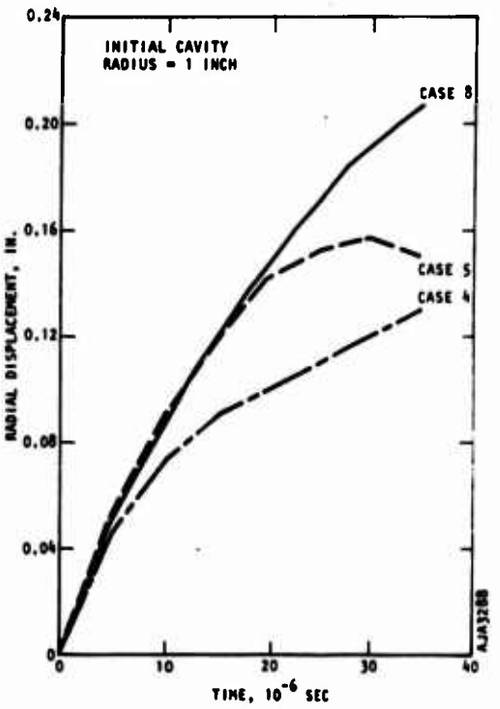

FIGURE 4-9. DISPLACEMENT OF CAVITY WALL, CASES 4, 5 AND 8

at late times. Figure 4-9 shows that displacements in Cases 5 and and 8 are identical at early times and do not begin to differ until after 20 μsec.

EFFECTIVENESS OF THE ITERATIVE TECHNIQUE

The reasons for resorting to the iterative technique described in Section 2 is that stress/strain coefficients and the cap parameters are implicit functions. Since there are many possible iterative techniques and the one presently used is somewhat complicated and time-consuming, it should at least be demonstrated to be accurate. Two demonstrations are made below. First, a sequence of shock loading stress states is examined at the end of each time step to see whether they lie on the appropriate cap.* Second, the time history of the cap parameter for the element adjacent to the cavity is studied to determine whether it varies with the integration time step (Δt).

*This is a more stringent test than showing the stresses to lie on the fracture surface (which can also be done) because the cap moves, whereas the fracture surface is constant.

In Case 8(a) ($\Delta t = 5 \times 10^{-8}$ sec), the value of the cap parameter κ in element 1 (adjacent to cavity) increases from zero to about 330 psi. The caps corresponding to shock loading and early unloading are defined by $0 < \kappa < 175$ psi and are shown in Figure 4-10. The number of time steps between successive caps varies from 1 ($0 \leq \kappa \leq 86$ psi) 5 to 7 (145 psi $\leq \kappa \leq 175$ psi). The maximum change in κ in any one step is about 120 percent ($\kappa = 31$ psi $\rightarrow \kappa = 70$ psi). Figure 4-10 shows that the stress state lies exactly on the cap up until $\kappa = 137$ psi and begins to drift off at higher values. The reason for this drifting is suggested in Figure 4-10, where, for $\kappa > 125$ psi, part of the cap lies above the fracture surface. The model should not behave in this way. The flaw in the model appears to lie in the functions contained in Equation 2-6. While R^2 increases very rapidly with J_{1F}, the term

$$\left[\frac{\partial f_1 / \partial J_1}{\partial f_1 / \partial \sqrt{J_2'}}\bigg|_F\right]^2$$

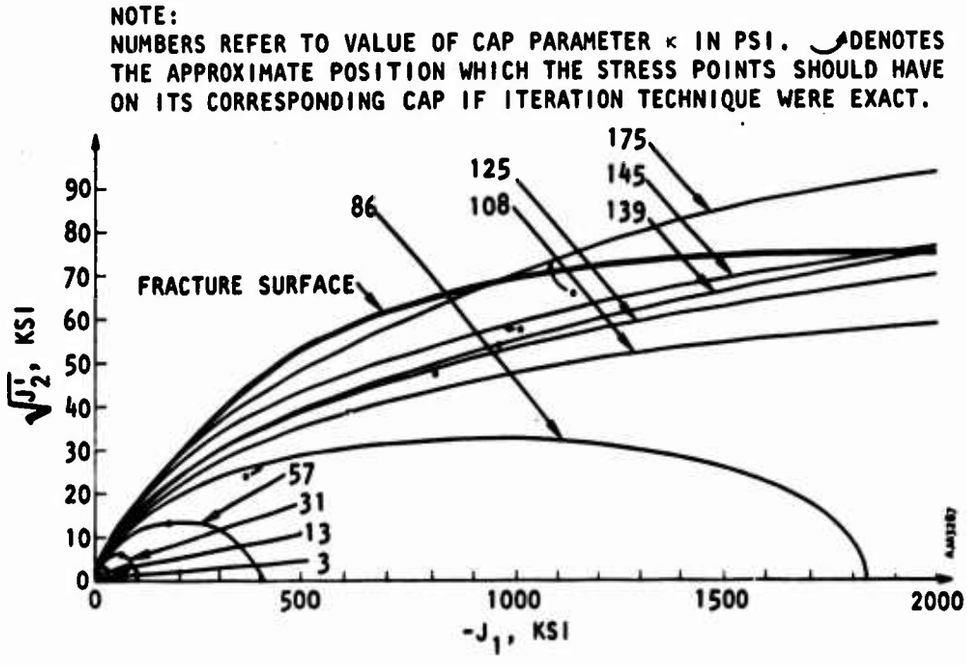

FIGURE 4-10. RELATIVE POSITIONS OF SUCCESSIVE STRESS POINTS AND CORRESPONDING CAPS, ELEMENT 1, CASE 8-a ($\Delta t = 5 \times 10^{-8}$ SEC)

should tend toward zero at the same rate. Thus $\sqrt{Q}$ (see Figure 2-1) would tend toward the von Mises limit of the fracture surface. Unfortunately, this balance is not achieved and $\sqrt{Q}$ exceeds the von Mises limit. The stress point eventually becomes constrained by the fracture surface and thus drifts away from the cap. The cap becomes larger and larger without any control being imposed by the fracture surface.

In spite of the apparent success of the present iterative technique, some difficulties remain as illustrated in Figure 4-11. In this figure the time histories of κ in Element 1 are shown for Cases 8(a) and 8(b). The only difference between the calculations is the integration time step which is 5×10^{-8} sec in 8(a) and 1.5×10^{-7} sec in 8(b). Case 8(a) uses the same time step as the previous seven cases and is considered to be superior to Case 8(b). One of the reasons Case 8(a) is considered to be superior is that the cap parameter is not required to undergo such large changes in one time step. Figure 4-11 shows that the present iterative procedure works about equally well for the large as for the small time step in the early times. As the cap approaches the yield surface however, and the model develops the flaw discussed above, the values of κ tend to diverge. This has some effect on response parameters of interest as reflected in the different displacements of the cavity wall, Figure 4-12.

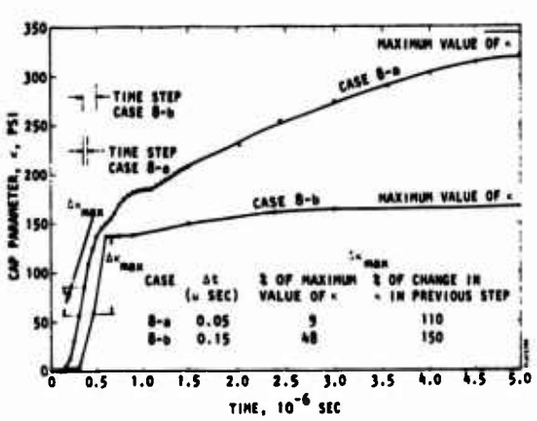

FIGURE 4-11. CHANGE IN SURFACE ($r/r_o = 1.015$) CAP PARAMETER κ WITH TIME AT CAVITY

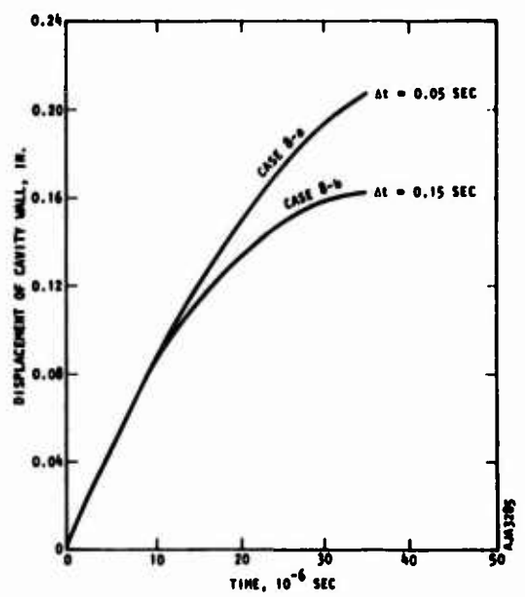

FIGURE 4-12. DISPLACEMENT OF CAVITY WALL IN CASE 8 FOR TWO DIFFERENT TIME STEPS

SECTION 5

SUMMARY AND CONCLUSIONS

Under conditions of spherical wave propagation, the capped model of rock is similar to the elastic, perfectly plastic models of Reference 2 with respect to wave shape and attenuation rate of peak stress. The amounts of energy absorbed in shear deformation and gained in volumetric dilatation are also close to those found for the models of Reference 2. The displacements of the cavity wall are significantly greater in the capped model than those in the previous models. The reason for the difference is not fully explained. Potential numerical difficulties associated with keeping the stress point on the cap or on the fracture surface during plastic deformation are noted. These are overcome in the present work by means of an iterative technique which uses an Euler formula for predicting and correcting the inelastic stress/strain coefficients until a stationary value of an arbitrary stress function is reached. A defect in the operation of the present capped model is noted, whereby it is possible for the cap to get outside the fracture surface.

The main conclusions of the present study are as follows:

a. In applications to spherical wave propagation, the capped model gives results which, in most respects, agree with the results from previous models.

b. An iterative technique which uses an Euler formula to predict and correct tangent moduli appears to be well-suited to finite element applications when the model contains implicit functions of the current plastic strain increments and the total stresses. The method can also be used for finite difference applications.

REFERENCES

1. Sandler, I., and F. L. Dimaggio, *Material Model for Rocks*, DASA 2595, Paul Weidlinger Consulting Engineer, October 1970.

2. Isenberg, J., et al., *Spherical Waves in Inelastic Materials*, DASA 2404, Agbabian-Jacobsen Associates, March 1970.

3. McKay, M. W., and C. S. Godfrey, *Study of Spherically Diverging Waves in Earth Media*, DASA 2223, Physics International Co., March 1969.